



# Morphology engineering and growth mechanism of ZnS nanostructures synthesized by solvothermal process

Sema Ebrahimi · Benyamin Yarmand

Received: 17 August 2019 / Accepted: 13 November 2019 / Published online: 30 November 2019  
© Springer Nature B.V. 2019

**Abstract** Zinc sulfide (ZnS) nanostructures with various morphologies play an imperative role in optoelectronic applications. In this study, different ZnS nanostructures with well-defined morphologies were synthesized in a controlled manner by a low-temperature solvothermal method using the binary solvent mixtures of ethylenediamine and water (EN/W). Controlling the content of EN and the growth temperature, ZnS nanostructures including nanoflowers, nanoflakes, nanorods, and hexagonal nanoplates were produced at a very low temperature ranging from 100 °C to 180 °C during short reaction times of 2 h and 6 h with excellent reproducibility. X-ray diffraction patterns of the nanostructures considerably revealed the single crystalline nature with a pure wurtzite phase of ZnS even at the low growth temperature having the average crystallite size in the range of 12.8–25.0 nm. The morphology evolution of the samples showed that there is a strong correlation between the morphologies of the ZnS nanostructures and the variations of both the growth temperature and reaction solvent. Based on the experimental results, a growth mechanism was also proposed for all the ZnS nanostructures with different morphologies. A sharp absorption band-edge was found for the ZnS nanostructures, in which the optical bandgap energy was laid ranging from 3.97 eV to 4.09 eV due to the quantum

confinement effect. All the samples featured a broad asymmetrical photoluminescence emission with multiple peaks, corresponding to excitonic and trapped luminescence centers. The effect of morphology on the optoelectronic performance resulted in a tremendous photoresponsivity and an excellent time-response switching behavior in UV region.

**Keywords** ZnS nanostructures · Morphology evolution · Growth mechanism · Solvothermal treatment · Low-temperature process

## Introduction

The materials engineering specified design and control of microstructures, dimensions, and morphologies of crystals have recently initiated great research interest, enabling the manifestation of their unprecedented properties and tailorable functions (Huang et al. 2003; Khomutov et al. 2003; Joshi and Schneider 2012). Semiconductor nanostructures with controlled dimension and morphology have drawn much attention as building blocks for the fabrication of optoelectronic devices (Tiwari and Dhoble 2016; Ebrahimi et al. 2019; Bacherikov et al. 2018; Xu et al. 2018). Zinc sulfide (ZnS) is a well-known wide-bandgap semiconductor with unique optoelectrical properties. It is applied in a wide range of applications such as photodetector (Fang et al. 2007a, b, c), lasers, and photocatalysts (Tiwari and Dhoble 2016; Fang et al. 2011a, b). For manipulating its optical properties and electrical

S. Ebrahimi · B. Yarmand (✉)  
Nanotechnology and Advanced Materials Department, Materials and Energy Research Center (MERC), Karaj, Iran  
e-mail: byarmand@merc.ac.ir

response, tuning the structure and morphology of that is desired during the synthetic process. ZnS can be found in two different polymorphic phases named zinc-blende and wurtzite phases, which show wide direct bandgaps about 3.72 eV and 3.77 eV, respectively. There is a free-energy difference of about  $13 \text{ kJ}\cdot\text{mol}^{-1}$  between both phases formed under ambient conditions (Fang et al. 2011a, b; Lixiong et al. 2015; Fang et al. 2011a, b; Fang et al. 2008; Liu et al. 2013; Mir et al. 2018; Qi et al. 2017). It is highly significant to control the crystalline phase and the surface morphology of the ZnS nanostructures for optoelectronic applications by precisely controlling the synthetic parameters and conditions affected their nucleation and growth.

Up to now, some chemical methods have been developed to synthesize the ZnS nanostructures with diverse morphologies such as the hydrothermal and/or solvothermal method. Generally, the solvothermal process is an extremely important method for the preparation of nanostructures with controlled phases and morphologies. It exhibits many benefits such as simplicity and tunability in equipment and the process, low temperature, and excellent yield in producing the homogeneous phases. It also offers several parameters to control the morphology due to the sensitivity of the reactions to the synthesis process parameters including the source of species, reaction time, growth temperature and the types of solvents (Demazeau 2010; Rao et al. 2004; Suchanek and Riman 2006; Fang et al. 2005; Fang et al. 2007a, b, c). The solvents play a significant role in the solvothermal process, which can influence the growth mechanism of ZnS nanostructures and thus determine their morphologies, sizes, and crystalline phases. Ethylenediamine (EN) have been widely utilized as a capping ligand for the synthesis of the ZnS nanostructures with various morphologies such as nanoflakes, nanorods, nanowires, and nanospheres (Acharya et al. 2013; Kole et al. 2014; Biswas and Kar 2008). Although different ZnS nanostructures have been produced, few studies have been reported on the flexible and tunable growth of the nanostructures within a simple fabrication system. In the case of EN-assisted synthesis, its molecules as structure-directing agents can react with  $\text{Zn}^{2+}$  cations and  $\text{S}^{2-}$  anions to design the ZnS nanostructures. However, to obtain the pure wurtzite phase from these compounds, a post-annealing treatment is frequently required to remove the EN molecules (Deng et al. 2002; Jang et al. 2008; Ouyang et al. 2003; Mosca et al. 2011). There is some more research on the preparation of the ZnS nanostructures using EN by the solvothermal route. Zhang et al., (Zhang

et al. 2012) developed an organic solvothermal strategy for the preparation of various morphologies of the ZnS including nanoparticles, nanobelts, and nanotetrapods and studied the evolution of the phase and morphology of the synthesized nanostructures. Kole et al., (Kole et al. 2014) expanded a simple and controllable hydrothermal process to synthesize the block-like, belt-like, spheroidal, and cuboidal shaped ZnS nanoparticles at the growth temperature of  $220 \text{ }^\circ\text{C}$  by adding ethylenediamine as the soft template to the synthetic solution. Han et al. (Han et al. 2016) attempted to produce ZnS nanoparticles, nanobelts, nanowires, and  $\text{ZnS}(\text{EN})_{0.5}$  complex structures by employing a one-pot solvothermal process using EN. Mendil et al. (Mendil et al. 2016) reported a microstructure and morphology evolution for the ZnS nanostructures solvothermal synthesized by applying a mixed solvent of EN and water. Therefore, it is still challenging to synthesize the pure wurtzite phase of the ZnS nanostructures directly by the solvothermal method at a low growth temperature and a short reaction time. This can only be done by finely controlling the synthetic conditions and parameters during the process and by introducing additional solvents or changing their concentrations.

Considering the different experimental conditions reported for producing a variety of morphologies of ZnS nanostructures, in this study, a controllable synthetic process was used for the preparation of ZnS nanostructures with the pure wurtzite phase based on using the binary EN/water solvent mixtures by a simple low-temperature solvothermal method. Changing the parameters, ZnS nanoflowers, nanoflakes, nanorods, and hexagonal nanoplates with a single wurtzite phase and good crystallinity were synthesized at very low growth temperatures from  $100 \text{ }^\circ\text{C}$  to  $180 \text{ }^\circ\text{C}$  and reaction times between 2 h and 6 h with excellent reproducibility. The effect of the growth temperature, types of solvents, and reaction time on the phase and morphology evolution as well as optoelectrical properties of ZnS nanostructures was investigated. Finally, a growth mechanism was proposed for the obtained morphologies.

## Experimental procedure

### Preparation of ZnS nanostructures

For the solvothermal treatment of ZnS nanocrystals, 0.2 M of zinc nitrate tetrahydrate ( $\text{Zn}(\text{NO}_3)_2\cdot 4\text{H}_2\text{O}$ , Aldrich, 98% purity) were dissolved into the solutions

containing the mixture of ethylenediamine (EN,  $C_2H_4(NH_2)_2$ , Merck, 98% purity) as a capping agent and deionized water at different volumetric ratios of EN/W. The detailed experimental conditions and the corresponding morphologies are presented in Table 1. An appropriate amount of thiourea ( $SC(NH_2)_2$ , Merck, > 98% purity) was then slowly added to the solutions and stirred vigorously for 30 min. The molar ratio of  $S^{2-}/Zn^{2+}$  was taken of about 3 for all the solutions. Thereafter, the prepared solutions were transferred into a 70 mL Teflon-lined stainless steel autoclave and sealed precisely. The autoclave was put into a pre-heated oven at different growth temperatures, followed by allowing to cool down to the room temperature, naturally. The obtained white precipitates were centrifuged and washed with deionized water and ethanol ( $C_2H_6O$ , Merck, > 65% purity) for several times, removing organic and inorganic pollutants. The final powder samples dried at 70 °C under vacuum conditions for 5 h.

#### Characterization techniques

High-resolution X-ray diffraction (XRD) (X'Pert PRO, MPD, NePANalytical) with Cu  $K\alpha$  radiation ( $\lambda = 1.54056 \text{ \AA}$ ) was used to study the crystalline structure of the samples, with the scanned angle ( $2\theta$ ) ranged between 20° and 80°. The morphology of the synthesized ZnS nanostructures was characterized using a field emission scanning electron microscope (FESEM, TESCAN, MIRA III). Transmittance spectra of samples were recorded using UV–visible spectrophotometer (Lambda25, Perkin Elmer) at the wavelength ranging from 300 to 700 nm. Photoluminescence (PL) has been performed at room temperature by applying the Perkin Elmer (LS-5) spectrometer with a helium-cadmium (He-Cd) laser having an excitation wavelength ( $\lambda_{ex}$ ) of 325 nm. The optoelectrical properties of the nanostructures were studied by changes

of the photocurrent by applying the voltage in the range from  $-5 \text{ V}$  to  $+5 \text{ V}$  under the dark and UV illumination (325 nm) conditions using a computer-controlled integrated source meter (Keithley 2400).

## Result and discussion

### Structural properties

The XRD patterns of ZnS nanostructures including nanoflowers, nanoflakes, nanorods, and hexagonal nanoplates synthesized by the solvothermal process during the reaction time of 2 h are shown in Fig. 1. Detailed phase structure of all the samples features diffraction peaks corresponded to (100), (002), (101), (107), (102), (110), (103), and (112) planes, revealing that all the synthesized ZnS nanostructures are well-crystallized to the wurtzite phase of ZnS (JCPDS card No. 01-089-2739) (Wang et al. 2009). However, the wurtzite structure is a high-temperature polymorph, which is stable at temperatures more than 1020 °C, the formation of that at a lower temperature can be considered due to the presence of the chelating solvent of EN (Acharya et al. 2013). Under the high-pressure condition, it can reduce the free energy difference between both phases of ZnS, wurtzite, and zinc-blende, which is resulted in the formation of the wurtzite phase at the lower temperature ranges (Fang et al. 2011a, b; Acharya et al. 2013). According to the literature, the formation of ZnS nanostructures in the presence of EN in the solvothermal treatment has been widely investigated and reported (Deng et al. 2002; Xi et al. 2008; Mi et al. 2010; Zhang et al. 2012; Han et al. 2016; Chen et al. 2003). Most of the studies found the formation of a complex  $(ZnS).En_{0.5}$  structure in the EN medium but not a pure wurtzite ZnS phase. Whereas, in this research, XRD

**Table 1** Experimental parameters and obtained morphologies of ZnS nanostructures during the solvothermal process

Series of Samples	Solvent EN/ W (Vol %)	Temperature (°C)	Time (h)	Morphology
1	75% EN/ W	100, 110, 120, 130, 140, 180	2, 6	Nanoflowers
2	50% EN/ W	110	2, 6	Nanoflakes
3	50% EN/ W	120, 130	2, 6	Nanoflakes and Nanorods
4	50% EN/ W	140	2, 6	Nanorods
5	50% EN/ W	180	2, 6	Hexagonal Nanoplates

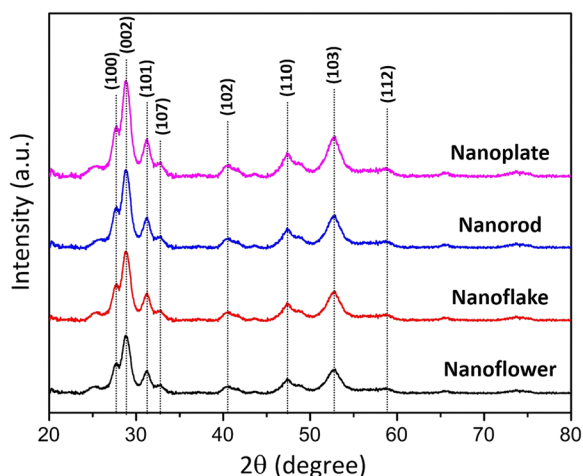


**Fig. 1** XRD patterns of ZnS nanostructures

patterns of all the synthesized ZnS nanostructures clearly reveal the direct formation of the pure wurtzite phase for ZnS nanostructures in the binary EN/W mixture, interestingly. The average crystallite size of the samples was estimated using the Scherrer formula of about 12.8, 17.3, 19.5, and 25.0 nm for the nanoflowers, nanoflakes, nanorods, and hexagonal nanoplates, respectively (Cullity and Stock 2001). The observed increase trend of the crystallite size of the ZnS nanostructures can be considered due to the influence of the synthetic parameters such as the concentration and type of solvent, growth temperature, and reaction time on the nucleation rate and growth mechanism of the nanostructures. Therefore, it can be suggested that the structural properties of the solvothermal synthesized ZnS nanostructures can be adjusted by modifying the synthesis process parameters in a controlled approach. Moreover, no evidence of the phase transformation and peak-shift was observed at different growth conditions, which can be associated with the formation of a high-quality wurtzite phase of nanosized ZnS structures. It has been also documented that the low-dimensional ZnS structures with wurtzite phase would be more thermodynamically stable than that of the zincblende one in the presence of EN solvent with chelating behavior. Herein, the surface energy of the nanosized wurtzite ZnS structures is lower than that of the zincblende. It can be due to the redesigning a large number of  $\text{Zn}^{2+}$  cations and  $\text{S}^{2-}$  anions on the surface of the wurtzite structure as a threefold coordinated ion with one unsaturated bond, resulting in the more stability of that to be formed during the process conditions (Senthilkumar and Selvi 2008; Fang et al. 2011a, b).

## Morphological evolution

### Nanoflowers

Figure 2 demonstrates the morphological evolution of ZnS nanoflowers synthesized at the various growth temperatures. Some irregular embryos of nanoflakes stacked together are observed in the mixed solvent of 75% EN/W at the low growth temperature of 100 °C for 2 h, which can be considered due to the self-aggregation of a large number of nanoparticles formed during the solvothermal reaction (Fig. 2a). By increasing the temperature, the size and number of formed nanoflakes were increased with many obvious edges, in which the rose-like nanostructures involving single-crystalline multilayer nanoflakes were apparently formed, as shown in Figs. 2b–f.

The time-dependent morphology evolution of the synthesized ZnS nanoflowers is presented in Fig. 3. Obviously, as the reaction time increased up to 6 h, the stacked nanoflowers with larger sizes were produced, consisting of numerous relative irregular nanoflakes.

The growth mechanisms of the formation of ZnS nanostructures can be complicated due to the involvement of different parameters according to the synthetic methods and various growth conditions. To explain the growth mechanism of the nanoflowers, a three-stage formation mechanism is proposed. As sketched in Fig. 4, the first stage indicates the nucleation and growth of the nanoflakes and the other can be attributed to the formation of the rose-like nanostructures. Based on the XRD patterns and FESEM images, the formation mechanism of ZnS nanoflowers can be described by an aggregation, dissolution-recrystallization process, and Ostwald ripening. Firstly, a large number of nanoparticles were formed by the solvothermal treatment of ZnS precursors in the EN/W mixed solvent media. Then, the produced nanoparticles self-aggregated into the nanoflakes to minimize the surface energy of the structure. Generally, when a moderate stability complex structure forms, it can be desirable for the formation of nanoflakes. Regarding the cumulative stability constants of EN molecules coordinated with  $\text{Zn}^{2+}$  ions, the crystallites can be difficultly grown in the epitaxial and one-dimensional way due to the higher stability of the complex structure, resulting in the predominantly formation of flake-like morphology for ZnS. The spontaneous growth of the nanoflakes was achieved by a dissolution-recrystallization process followed by the Ostwald ripening in the solvothermal route, in which

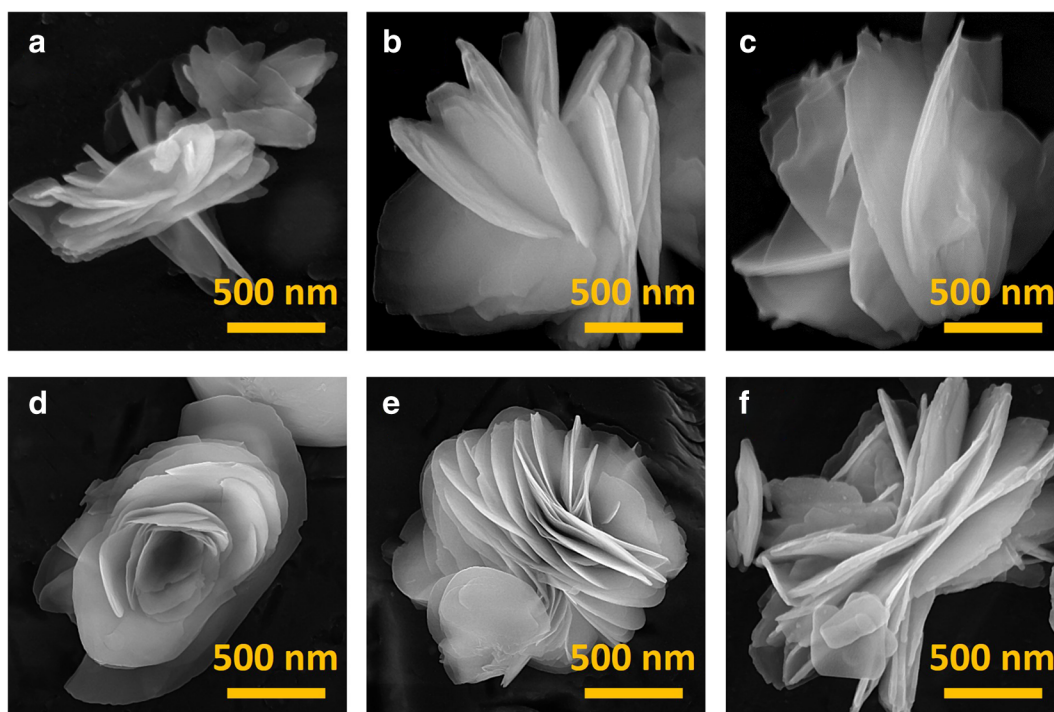


**Fig. 2** FESEM images of ZnS nanoflowers during the reaction time of 2 h at the different growth temperature of (a) 100 °C, (b) 110 °C, (c) 120 °C, (d) 130 °C, (e) 140 °C, and (f) 180 °C

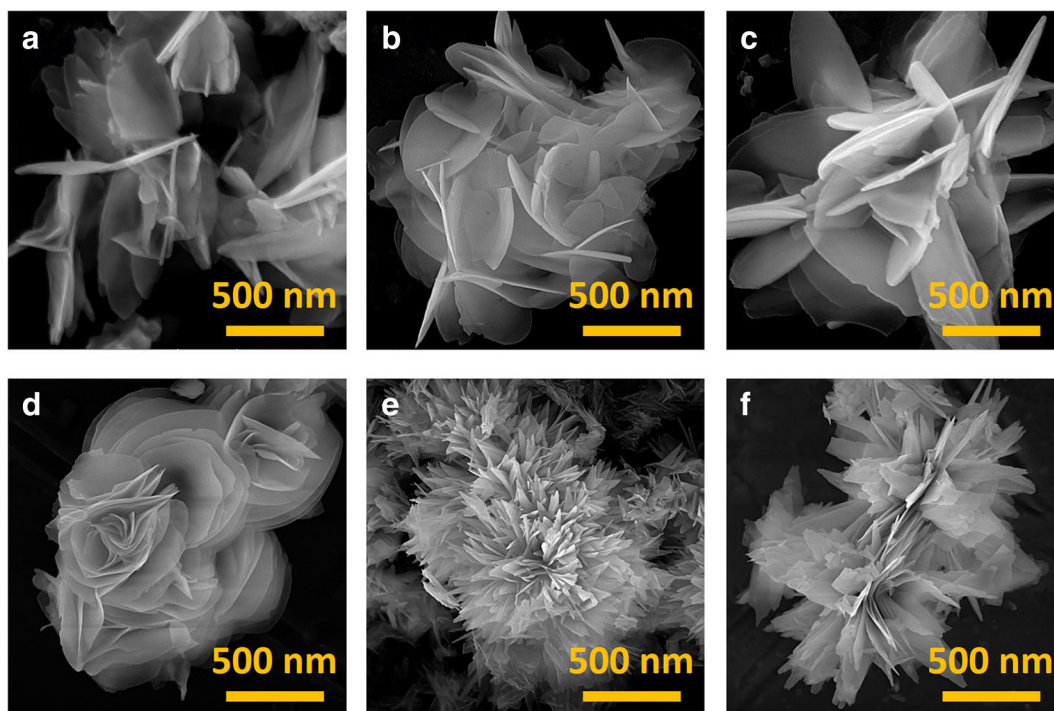


**Fig. 3** FESEM images of ZnS nanoflowers prepared during the reaction time of 6 h at the different growth temperature of (a) 100 °C, (b) 110 °C, (c) 120 °C, (d) 130 °C, (e) 140 °C, and (f) 180 °C

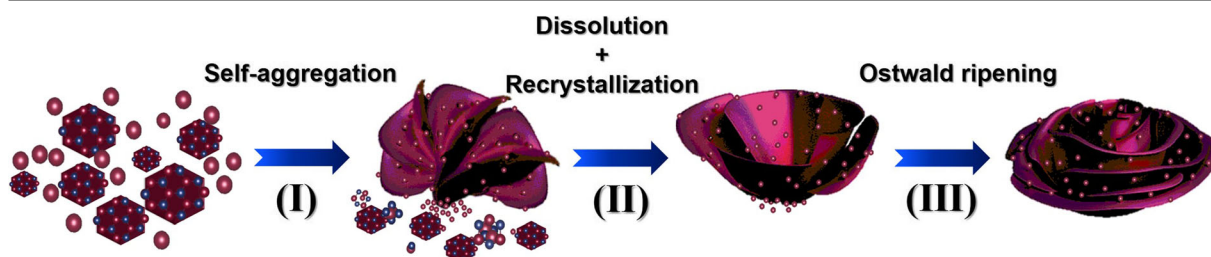


**Fig. 4** Schematic illustration of the formation of ZnS nanoflowers

the nanoflakes are gradually grown up and finally self-assembled into the rose-like nanoflowers. By increasing the reaction time, the size of the nanoflowers grew larger with a bunch of stacked nanoflakes standing on the surfaces (Wang et al. 2012a, b; Tiwari and Dhoble 2016).

#### *Nanoflakes and nanorods*

Since the morphology of nanostructures is sensitive to the reaction solvent, the effect of different solvent mixtures on the morphology of ZnS nanostructures will be discussed here. The FESEM images of ZnS nanoflakes and nanorods formed in 50% EN/W mixed solvent at various growth temperatures during the reaction time of 2 h are shown in Figure 5. At the temperature of 110 °C, the samples reveal flake-like morphology with a stacked structure composed of several aligned nanoflakes. By increasing the temperature to 120 °C and 130 °C, ZnS nanostructures recrystallized to produce nanorods in addition to the nanoflakes and at the growth temperature of about 140 °C, the morphology of the ZnS nanostructures is almost changed to the nanorods. By mixing EN and water in equal volumetric ratio as a reaction solvent, the nanostructures will be arranged by nanoflakes to form a complex ZnS(EN)<sub>0.5</sub> layered structure, which can be attributed to the binding capacity and Lewis base of the EN and Zn<sup>2+</sup> cations (Wang et al. 2012a, b; Yue et al. 2006). Particularly, in a mixed EN/W solvent, owing to the presence of two lone pairs of electrons associated with two nitrogen atoms in EN molecule, it can act as an active bidentate ligand to cationic Zn<sup>2+</sup> ions. In the presence of the S<sup>2-</sup> anions, a complex layered structure can be produced by alternate stacking of EN and ZnS flakes (Biswas and Kar 2008). As the growth temperature rising, volatile amine molecules come out of the layered structure at a suitable temperature, resulting in the destruction of the nanoflakes and the production of the ZnS nanorods (Tiwari and Dhoble 2016; Senthilkumar and Selvi 2008; Wang et al. 2012a, b;

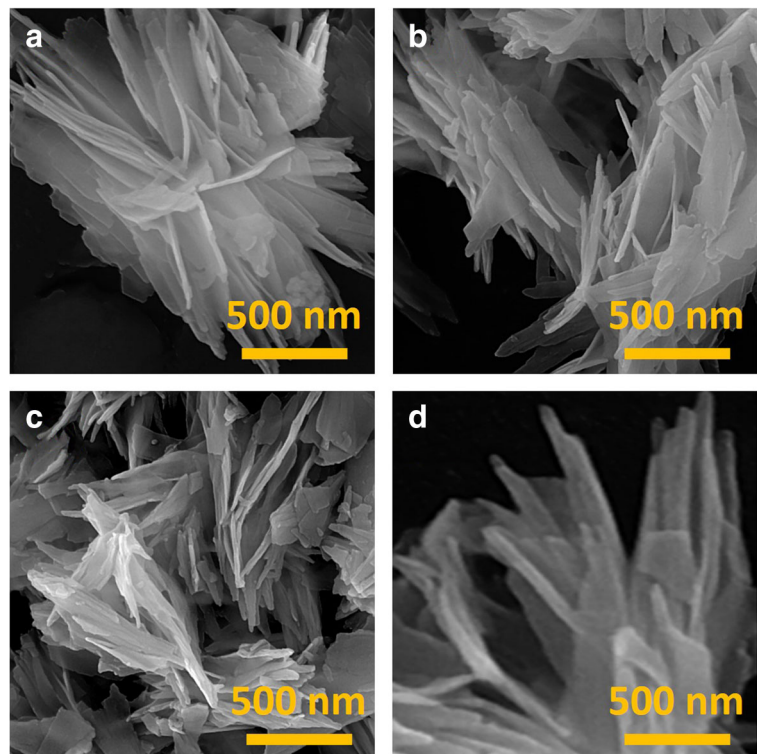
Yue et al. 2006). Vividly, due to the faster growth rate of the (002) crystal plane of ZnS with maximum surface energy than that of the EN-passivated (010) plane, a one-dimensional rod-like morphology assembled with a wurtzite phase along the vertical direction of c-axis is most desirable morphology to produce, as discussed in the XRD section. Therefore, EN can modulate the growth pattern of nanostructures by acting as both structure-directing and surface-passivating coordination agent and thus controlling their morphologies (Tiwari and Dhoble 2016; Mendil et al. 2016; Han et al. 2016). As illustrated in Fig. 6, a relevant growth mechanism for the formation of nanoflakes and nanorods under the experimental conditions can be suggested as a three-step-process including self-aggregation, recrystallization process of nanoparticles and finally lined up the structures by Oriented Attachment, followed by the Ostwald ripening growing mechanism. The anisotropic growth mechanism and the morphology evolution of the ZnS nanostructures synthesized by the solvothermal/hydrothermal method have been profoundly elucidated recently by Wang et al. (Wang et al. 2012a, b), Yue et al. (Yue et al. 2006), Mendil et al. (Mendil et al. 2016), and Fang et al. (Fang et al. 2007a, b, c).

Considering the effect of reaction time on the morphology evaluation of the nanoflakes and nanorods shown in Fig. 7, it can be deduced that the growth mechanism of the ZnS nanostructures can only be affected either by thermal agitation or introducing some foreign solvents to the system such as water and employing the benefits of organic/water solvent mixtures (Biswas and Kar 2008). However, by increasing the reaction time, the size and number of the synthesized ZnS nanostructures could be varied and enlarged to some extent.

#### *Hexagonal nanoplates*

The FESEM images of the ZnS nanostructures synthesized in 50% EN/W mixed solvent media at the growth

**Fig. 5** FESEM images of ZnS nanoflakes and nanorods during the reaction time of 2 h at the different growth temperature of (a) 110 °C, (b) 120 °C, (c) 130 °C, and (d) 140 °C



temperature of 180 °C are indicated in Fig. 8. According to Fig. 8a, during the reaction time of 2 h, the quasi-hexagonal nanoplates of ZnS were produced. Non-uniform and the quasi hexagonal-like morphology of ZnS nanoplates was obtained due to the low reaction time, which could not provide suitable conditions for the growth and formation of hexagonal nanoplates. To study the effect of reaction time on the morphology and size of ZnS nanoplates, the FESEM image of the ZnS nanostructures prepared during the reaction time of about 6 h is shown in Fig. 8b. By increasing the time, large numbers of uniform ZnS hexagonal nanoplates were formed with almost the same orientation, in which the size of the plate-like nanostructures was larger than that of the sample synthesized at 2 h (Mendil et al. 2016; Shakouri-Arani and Salavati-Niasari 2014). Figure 9

illustrates the possible growth mechanism of the hexagonal nanoplates. In the reaction system containing the equal mixed solvent of EN/W at the high growth temperature, numerous ZnS nanoparticles were initially formed. Then, the nanoparticles spontaneously aggregated to large particles to reduce the surface energies. After obtaining a critical size during Ostwald ripening, the nanoparticles act as the building blocks for the crystallization through the Oriented-Attachment mechanism. In order that the nanoparticles formed with structurally similar surfaces attach each other at their high-energy interfaces to achieve full coordination and thereby minimize the surface energy corresponded to the unsatisfied bonds. Finally, the hexagonal plate-like architectures can be formed based on the similar growth rate of the crystallite planes with different impacts at the high growth

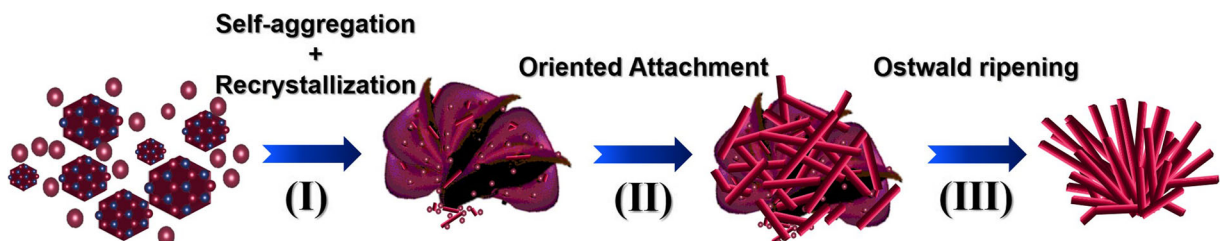
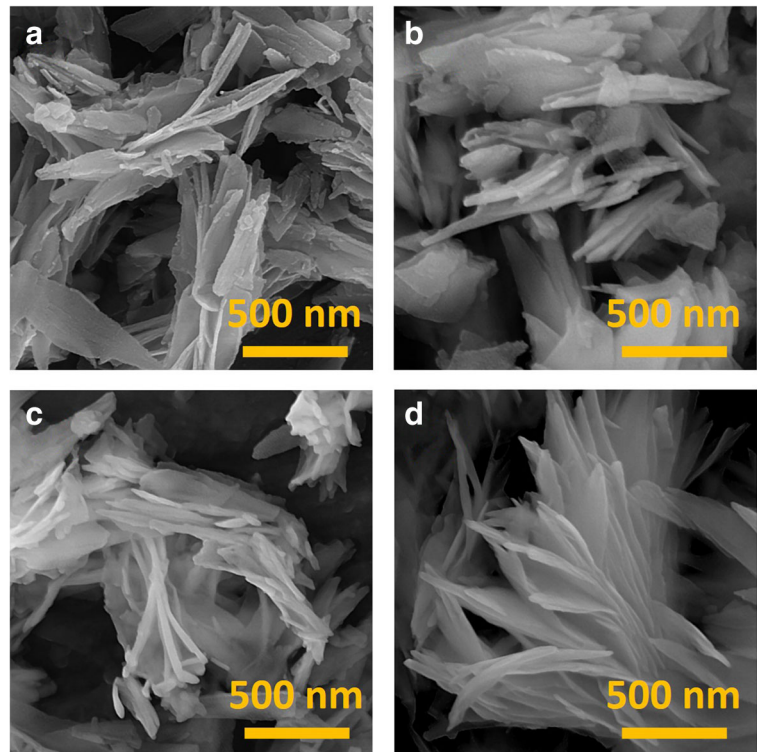


**Fig. 6** Schematic illustration of the formation of ZnS nanoflowers and nanorods

**Fig. 7** FESEM images of ZnS nanoflakes and nanorods during the reaction time of 6 h at the different growth temperature of (a) 110 °C, (b) 120 °C, (c) 130 °C, and (d) 140 °C



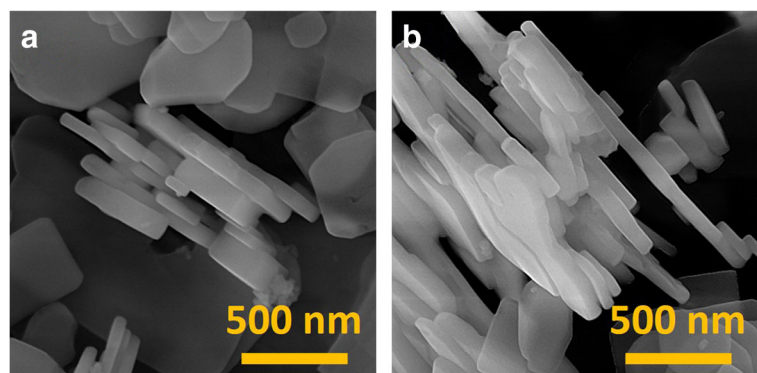
temperature. Consequently, the ethylenediamine as a capping agent can play a key role in the solvothermal process, which signifies that the progress can affect the selective nucleation and mechanism of growth in the formation of various compounds.

#### Optical properties

To shed light on how the various morphologies of the ZnS nanostructures can influence the optical properties, the optical absorption spectra and PL of the synthesized ZnS nanostructures are presented in Fig. 10. Regarding the optical absorption spectra, all the ZnS nanostructures

pointed out an optical absorption band-edge in the UV region of the spectrum. Interestingly, there are two peaks existing in the absorption spectra of the nanostructures, in which a modest peak is located around 310 nm along with a shoulder peak at about 318 nm. An observed sharp optical absorption band-edges for all the samples can be ascribed to the high specific surface area and superior light-harvesting ability of the ZnS nanostructures. Further, it can be found that, as the growth temperature increased and the reaction proceeded up to producing the hexagonal nanoplates, the two absorption peaks became stronger; while the position of the two peaks experienced no significant changes. This

**Fig. 8** FESEM images of ZnS hexagonal nanoplates at the growth temperature of 180 °C during the reaction time of (a) 2 h and (b) 6 h.





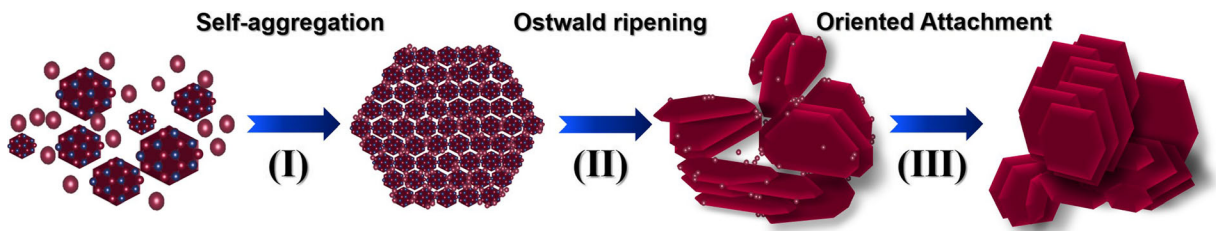


**Fig. 9** Schematic illustration of the formation of ZnS hexagonal nanoplates

observation can be considered due to the growth of high-crystalline-quality nanostructures at high temperatures, as proved by XRD. The optical bandgap energy of all the samples was determined by applying a known Tauc's equation near the absorption band-edge (Varshni 1967; Ebrahimi et al. 2019). The values of bandgap energy were estimated at about 4.09, 4.05, 4.02, and 3.97 for the nanoflowers, nanoflakes, nanorods, and hexagonal nanoplates, respectively. A slight narrowing of the optical bandgap energy can be attributed to the size variation, changes of the morphologies, and thus the specific surface area of the two- and one-dimensional ZnS nanostructures as a function of solvothermal growth conditions. However, the obtained bandgap energies of the ZnS nanostructures are at the higher values than that of the bulk ZnS, which can be assigned to their nanocrystalline nature and nanometer sizes laid in the quantum confinement range (Chandran et al. 2010).

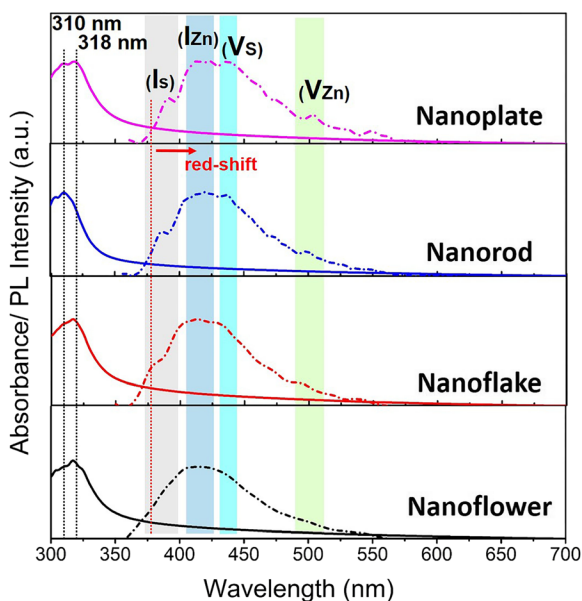


**Fig. 10** UV-Visible absorption (left) and PL spectra (right) of ZnS nanostructures

These findings are consistent perfectly with the other related studies (Li et al. 2004a, b; Biswas and Kar 2008; Li et al. 2008).

As shown in Fig. 10, the PL spectra of ZnS nanostructures is asymmetrical with multiple peaks, because it can be affected by the experimental and synthetic conditions as well as the size and morphology of the samples (Li, Li, et al. 2004; Li, Pradhan, et al. 2004; Biswas and Kar 2008). The appearance of the appeared emission peaks can be attributed to the transition of donor-acceptor pairs. For all the ZnS nanostructures, four emission peaks in their PL spectrum can be observed, which are related to their excitonic and trapped luminescence centers. The emission peaks for all the samples are positioned at about 374, 408, 430, and 491 nm, which can be assigned to the interstitial sulfur lattice defects, interstitial zinc lattice defects, sulfur vacancies, and zinc vacancies, respectively (Ebrahimi, Yarmand, and Naderi 2019; Viswanath et al. 2014). It is obvious that the PL emissions arisen from the excitonic luminescence centers are sharp and locates near the optical absorption edge of the samples, whereas the emissions corresponded to the trapped centers are broad and relatively Stokes-shifted (O'neil et al. 1990). A relative difference in the intensity and position of the PL emissions of the samples refers to their different morphologies and sizes during the various synthetic conditions.

#### Optoelectronic performance

The photoelectrical properties of the ZnS nanostructures were investigated in the mode of metal-semiconductor-metal (MSM) photodetector under the dark and UV illumination. The I-V curves of the ZnS nanostructures with different morphologies are shown in Fig. 11a. All the samples exhibit a good rectification behavior in the dark and high photocurrent response under UV exposure. Considering the effect of various morphologies on the optoelectrical properties of the ZnS nanostructures,

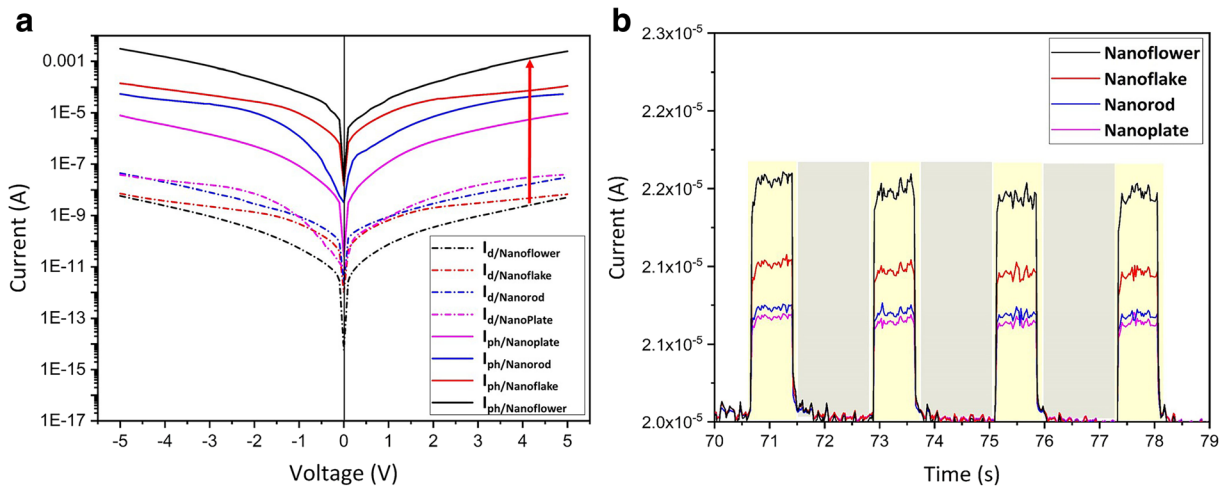


**Fig. 11** (a) I–V curves and (b) time-response switching of ZnS nanostructures

an obvious decrease in the dark currents of the samples in the order of hexagonal nanoplates, nanorods, nanoflakes, and nanoflowers was observed, through which the noise-to-signal ratio can be significantly reduced in the ZnS-based photodetectors. Upon the UV illumination, the ZnS nanoflowers indicate a tremendous photoresponsivity and sensitivity compared to the others, which can be considered due to the nanosized structures and surface cavities and excellent optical properties of the nanoflowers, harvesting more photons and producing more generated photocurrent.

The time response behavior of the ZnS nanostructures was depicted in Fig. 11b. The samples show excellent reproducibility and stability under UV illumination at the applied voltage of 5 V. The generated photocurrent was found to considerably enhance for the ZnS nanoflowers, as discussed in the previous section. The response time of the samples followed a quickly switching optical signal, in which the response rise and decay times are defined as the time taken for the photocurrent to increase up to 90% of the value or vice versa, respectively. The rise/decay times were estimated of about 12.5/17.9, 16.2/24.6, 21.7/28.3, and 29.1/35.0 s for the ZnS nanoflowers, nanoflakes, nanorods, and hexagonal nanoplates, respectively. Accordingly, the lowest value of time response switching was found for the ZnS nanoflowers, which is offered the high-speed photo switching characteristics for the ZnS-based photodetectors (Liang et al. 2012; Wang et al. 2012a, b; Zheng et al. 2010a, b; Xu et al. 2018). Therefore, it can be noted that the grown ZnS nanostructures with different morphologies of nanoflowers, nanoflakes, nanorods,

and hexagonal nanoplates can feature large potential applications in optoelectronic devices such as nanosensors, field-effect transistors, LEDs, nanosized catalysts owing to their unprecedented structural and optical properties as mentioned above.

## Conclusion

In the present work, a simple and cost-effective low-temperature solvothermal method was designed to synthesize the single crystalline, wurtzite ZnS nanostructures with different morphologies using a binary mixed solvent of EN and water. Driven by ZnS crystal planes anisotropy and obeying the crystal growth theories, it was found that four types of morphologies including nanoflowers, nanoflakes, nanorods, and hexagonal nanoplates can be tailored for ZnS nanostructures by controlling the growth temperature, reaction time and varying the contents of EN in the reaction solvent. By studying the morphology evolution of the synthesized ZnS nanostructures, a growth mechanism was proposed for all the samples based on the self-aggregation, dissolution-recrystallization process, Ostwald ripening, and Oriented Attachments principles. The optical absorption of the nanostructures showed two peaks located at 310 nm and 318 nm having a strong absorption band-edge, in which the optical bandgap energy was determined of about 4.09, 4.05, 4.02, and 3.97 eV for the nanoflowers, nanoflakes, nanorods, and hexagonal nanoplates, respectively. The PL spectra of all the samples also revealed four emission peaks at around 374,

408, 430, and 491 nm, which can be corresponded to the excitonic and trapped luminescence centers of the ZnS. Although several low-temperature hydrothermal and/or solvothermal route of ZnS nanostructures have been recently reported, our low-temperature process allows producing ZnS nanostructures of various morphologies in a well-controlled approach, which can be used as building blocks for future optoelectronic devices owing to their high photoresponsivity and excellent time-response switching characteristics.

**Acknowledgment** Authors are grateful to Iran National Science Foundation (INSF) for providing financial support to undertake this work by Grant No. 95822972.

#### Compliance with ethical standards

**Conflict of interest** The authors declare that they have no conflict of interest.

#### References

- Acharya SA, Maheshwari N, Tatikondewar L, Kshirsagar A, Kulkarni SK (2013) Ethylenediamine-mediated wurtzite phase formation in ZnS. *Crystal Growth & Design* 13: 1369–1376
- Bacherikov YY, Lytvyn PM, Okhrimenko OB, Zhuk AG, Kurichka RV, Doroshkevich AS (2018) Surface potential of meso-dimensional ZnS: Mn particles obtained using SHS method. *Journal of Nanoparticle Research* 20:316
- Biswas S, Kar S (2008) Fabrication of ZnS nanoparticles and nanorods with cubic and hexagonal crystal structures: a simple solvothermal approach. *Nanotechnology* 19:045710
- Chandran A, Francis N, Jose T, George KC (2010) Synthesis, structural characterization and optical bandgap determination of ZnS nanoparticles. *Acad Rev* 17:17–21
- Chen X, Xu H, Xu N, Zhao F, Lin W, Lin G, Yunlong F, Huang Z, Wang H, Mingmei W (2003) Kinetically controlled synthesis of wurtzite ZnS nanorods through mild thermolysis of a covalent organic–inorganic network. *Inorganic Chemistry* 42:3100–3106
- Cullity, BD, and SR Stock. 2001. "Elements of X-ray diffraction third edition prentice hall upper saddle river." In.: NJ.
- Demazeau G (2010) Solvothermal processes: definition, key factors governing the involved chemical reactions and new trends. *Zeitschrift für Naturforschung B* 65:999–1006
- Deng Z-X, Cheng W, Sun X-M, Li Y-D (2002) Structure-directing coordination template effect of ethylenediamine in formations of ZnS and ZnSe nanocrystallites via solvothermal route. *Inorganic Chemistry* 41:869–873
- Ebrahimi S, Yarmand B, Naderi N (2019) Enhanced optoelectrical properties of Mn-doped ZnS films deposited by spray pyrolysis for ultraviolet detection applications. *Thin Solid Films* 676:31–41
- Fang X-S, Ye C-H, Zhang L-D, Wang Y-H, Yu-Cheng W (2005) Temperature-controlled catalytic growth of ZnS nanostructures by the evaporation of ZnS nanopowders. *Advanced Functional Materials* 15:63–68
- Fang, Xiaosheng, Yoshio Bando, Changhui Ye, and Dmitri Golberg. 2007a. 'Crystal orientation-ordered ZnS nanobelt quasi-arrays and their enhanced field-emission', *Chemical Communications*: 3048–50.
- Fang X, Bando Y, Ye C, Shen G, Golberg D (2007b) Shape- and size-controlled growth of ZnS nanostructures. *The Journal of Physical Chemistry C* 111:8469–8474
- Fang XS, Yoshio B, Shen GZ, Ye CH, Gautam UK, Costa PMFJ, Zhi CY, Tang CC, Golberg D (2007c) Ultrafine ZnS nanobelts as field emitters. *Advanced Materials* 19:2593–2596
- Fang X, Gautam UK, Bando Y, Dierre B, Sekiguchi T, Golberg D (2008) Multiangular branched ZnS nanostructures with needle-shaped tips: potential luminescent and field-emitter nanomaterial. *The Journal of Physical Chemistry C* 112: 4735–4742
- Fang X, Wu L, Linfeng H (2011a) ZnS nanostructure arrays: a developing material star. *Advanced Materials* 23:585–598
- Fang X, Zhai T, Gautam UK, Li L, Wu L, Bando Y, Golberg D (2011b) ZnS nanostructures: from synthesis to applications. *Progress in Materials Science* 56:175–287
- Han S, Liu W, Sun K, Xiaotao Z (2016) Experimental evidence of ZnS precursor anisotropy activated by ethylenediamine for constructing nanowires and single-atomic layered hybrid structures. *CrystEngComm* 18:2626–2631
- Huang X, Li J, Zhang Y, Mascarenhas A (2003) From 1D chain to 3D network: tuning hybrid II–VI nanostructures and their optical properties. *Journal of the American Chemical Society* 125:7049–7055
- Jang JS, Yu C-J, Choi SH, Ji SM, Kim ES, Lee JS (2008) Topotactic synthesis of mesoporous ZnS and ZnO nanoplates and their photocatalytic activity. *Journal of Catalysis* 254: 144–155
- Joshi RK, Schneider JJ (2012) Assembly of one dimensional inorganic nanostructures into functional 2D and 3D architectures. Synthesis, arrangement and functionality. *Chemical Society Reviews* 41:5285–5312
- Khomutov GB, Kislov VV, Gainutdinov RV, Gubin SP, Obydenov AY, Pavlov SA, Sergeev-Cherenkov AN, Soldatov ES, Tolstikhina AL, Trifonov AS (2003) The design, fabrication and characterization of controlled-morphology nanomaterials and functional planar molecular nanocluster-based nanostructures. *Surface science* 532:287–293
- Kole AK, Tiwary CS, Kumbhakar P (2014) Morphology controlled synthesis of wurtzite ZnS nanostructures through simple hydrothermal method and observation of white light emission from ZnO obtained by annealing the synthesized ZnS nanostructures. *Journal of Materials Chemistry C* 2: 4338–4346
- Li LS, Pradhan N, Wang Y, Peng X (2004a) High quality ZnSe and ZnS nanocrystals formed by activating zinc carboxylate precursors. *Nano letters* 4:2261–2264
- Li Y, Li X, Yang C, Li Y (2004b) Ligand-controlling synthesis and ordered assembly of ZnS nanorods and nanodots. *The Journal of Physical Chemistry B* 108:16002–16011

- Li Z, Wang J, Xu X, Ye X (2008) The evolution of optical properties during hydrothermal coarsening of ZnS nanoparticles. *Materials letters* 62:3862–3864
- Liang Y, Liang H, Xiao X, Hark S (2012) The epitaxial growth of ZnS nanowire arrays and their applications in UV-light detection. *Journal of Materials Chemistry* 22:1199–1205
- Liu H, Hu L, Watanabe K, Hu X, Dierre B, Kim B, Sekiguchi T, Fang X (2013) Cathodoluminescence modulation of ZnS nanostructures by morphology, doping, and temperature. *Advanced Functional Materials* 23:3701–3709
- Lixiong Y, Wang D, Jianfeng H, Liyun C, Haibo O, Wu J, Xiang Y (2015) Microwave hydrothermal synthesis and photocatalytic activities of morphology-controlled ZnS crystallites. *Ceramics International* 41:3288–3292
- Mendil R, Ben Ayadi Z, Djessas K (2016) Effect of solvent medium on the structural, morphological and optical properties of ZnS nanoparticles synthesized by solvothermal route. *Journal of Alloys and Compounds* 678:87–92
- Mi L, Han M, Li Z, Wang Y, Shen C, Zheng Z (2010) Transformation of a zinc inclusion complex to wurtzite ZnS microflowers under solvothermal conditions. *Crystal Research and Technology* 45:973–976
- Mir IA, Alam H, Priyadarshini E, Meena R, Rawat K, Rajamani P, Rizvi MS, Bohidar HB (2018) Antimicrobial and biocompatibility of highly fluorescent ZnSe core and ZnSe@ ZnS core-shell quantum dots. *Journal of Nanoparticle Research* 20:174
- Mosca R, Ferro P, Calestani D, Nasi L, Besagni T, Licci F (2011) Solvothermal synthesis of ZnS [C<sub>2</sub>H<sub>4</sub>(NH<sub>2</sub>)<sub>2</sub>] 0.5 nanosheets. *Crystal Research and Technology* 46:818–822
- O'neil M, Marohn J, McLendon G (1990) Dynamics of electron-hole pair recombination in semiconductor clusters. *Journal of Physical Chemistry* 94:4356–4363
- Ouyang, Xiang, Tsung-Yen Tsai, Dong-Hwang Chen, Qi-Jie Huang, Wu-Hsun Cheng, and Abraham Clearfield. 2003. 'Ab initio structure study from in-house powder diffraction of a novel ZnS (EN) 0.5 structure with layered wurtzite ZnS fragment'. *Chemical Communications*: 886-87.
- Qi S, Zhang M, Guo X, Yue L, Wang J, Shao Z, Xin B (2017) Controlled extracellular biosynthesis of ZnS quantum dots by sulphate reduction bacteria in the presence of hydroxypropyl starch as a mediator. *Journal of Nanoparticle Research* 19: 212
- Rao, CNR, Achim Muller, and Anthony K Cheetham. 2004. *The chemistry of nanomaterials* (Wiley Online Library).
- Senthilkumaar, S, and R Thamiz Selvi. 2008. 'Synthesis and characterization of one dimensional ZnS nanorods', *synthesis and reactivity in inorganic, metal-organic, and nano-metal chemistry*, 38: 710-15.
- Shakouri-Arani M, Salavati-Niasari M (2014) Synthesis and characterization of wurtzite ZnS nanoplates through simple solvothermal method with a novel approach. *Journal of industrial and engineering chemistry* 20: 3179–3185
- Suchanek WL, Riman RE (2006) Hydrothermal synthesis of advanced ceramic powders. In: In *Advances in Science and Technology*, 184-93. Publ, Trans Tech
- Tiwari A, Dhoble SJ (2016) Critical analysis of phase evolution, morphological control, growth mechanism and photophysical applications of ZnS nanostructures (zero-dimensional to three-dimensional): a review. *Crystal Growth & Design* 17:381–407
- Varshni, YP. 1967. 'Band-to-band radiative recombination in groups IV, VI, and III-V semiconductors (I)', *physica status solidi (b)*, 19: 459-514.
- Viswanath R, Bhojya Naik HS, Yashavanth Kumar GS, Prashanth Kumar PN, Arun Kumar G, Praveen R (2014) EDTA-assisted hydrothermal synthesis, characterization and photoluminescent properties of Mn<sup>2+</sup>-doped ZnS. *Journal of Luminescence* 153:446–452
- Wang H, Chen Z, Cheng Q, Yuan L (2009) Solvothermal synthesis and optical properties of single-crystal ZnS nanorods. *Journal of Alloys and Compounds* 478:872–875
- Wang L, Dai J, Liu X, Zhu Z, Huang X, Pingwei W (2012a) Morphology-controlling synthesis of ZnS through a hydrothermal/solvothermal method. *Ceramics International* 38:1873–1878
- Wang X, Xie Z, Huang H, Liu Z, Chen D, Shen G (2012b) Gas sensors, thermistor and photodetector based on ZnS nanowires. *Journal of Materials Chemistry* 22:6845–6850
- Xi G, Wang C, Wang X, Zhang Q, Xiao H (2008) From ZnS  $\infty$  nanosheets to wurtzite ZnS nanorods under solvothermal conditions. *The Journal of Physical Chemistry C* 112:1946–1952
- Xu X, Li S, Chen J, Cai S, Long Z, Fang X (2018) Design principles and material engineering of ZnS for optoelectronic devices and catalysis. *Advanced Functional Materials* 28: 1802029
- Yue GH, Yan PX, Yan D, Liu JZ, Qu DM, Yang Q, Fan XY (2006) Synthesis of two-dimensional micron-sized single-crystalline ZnS thin nanosheets and their photoluminescence properties. *Journal of crystal growth* 293:428–432
- Zhang Y, Liu W, Wang R (2012) From ZnS nanoparticles, nanobelts, to nanotetrapods: the ethylenediamine modulated anisotropic growth of ZnS nanostructures. *Nanoscale* 4: 2394–2399
- Zheng XJ, Chen YQ, Zhang T, Jiang CB, Yang B, Yuan B, Mao SX, Li W (2010a) A photoconductive semiconductor switch based on an individual ZnS nanobelt. *Scripta Materialia* 62: 520–523
- Zheng XJ, Chen YQ, Zhang T, Yang B, Jiang CB, Yuan B, Zhu Z (2010b) Photoconductive semiconductor switch based on ZnS nanobelts film. *Sensors and Actuators B: Chemical* 147:442–446

**Publisher's note** Springer Nature remains neutral with regard to jurisdictional claims in published maps and institutional affiliations.